

The pressure tensor across a liquid-vapour interface

Cite as: J. Chem. Phys. **149**, 044705 (2018); <https://doi.org/10.1063/1.5020991>

Submitted: 29 December 2017 . Accepted: 21 May 2018 . Published Online: 30 July 2018

Carlos Braga, Edward R. Smith , Andreas Nold , David N. Sibley , and Serafim Kalliadasis 



View Online



Export Citation



CrossMark

ARTICLES YOU MAY BE INTERESTED IN

[A new approach for the prediction of partition functions using machine learning techniques](#)

The Journal of Chemical Physics **149**, 044118 (2018); <https://doi.org/10.1063/1.5037098>

[Mesoscopic coarse-grained representations of fluids rigorously derived from atomistic models](#)

The Journal of Chemical Physics **149**, 044104 (2018); <https://doi.org/10.1063/1.5039738>

[The Statistical Mechanical Theory of Surface Tension](#)

The Journal of Chemical Physics **17**, 338 (1949); <https://doi.org/10.1063/1.1747248>

The Journal
of Chemical Physics

2018 EDITORS' CHOICE

READ NOW!



The pressure tensor across a liquid-vapour interface

Carlos Braga,^{1,a)} Edward R. Smith,^{1,b)} Andreas Nold,^{1,2,c)} David N. Sibley,^{3,d)} and Serafim Kalliadasis^{1,e)}

¹Department of Chemical Engineering, Imperial College London, London SW7 2AZ, United Kingdom

²Theory of Neural Dynamics, Max Planck Institute for Brain Research, 60438 Frankfurt a. M., Germany

³Department of Mathematical Sciences, Loughborough University, Leicestershire LE11 3TU, United Kingdom

(Received 29 December 2017; accepted 21 May 2018; published online 30 July 2018)

Inhomogeneous fluids exhibit physical properties that are neither uniform nor isotropic. The pressure tensor is a case in point, key to the mechanical description of the interfacial region. Kirkwood and Buff and, later, Irving and Kirkwood, obtained a formal treatment based on the analysis of the pressure across a planar surface [J. G. Kirkwood and F. P. Buff, *J. Chem. Phys.* **17**(3), 338 (1949); J. H. Irving and J. G. Kirkwood, *J. Chem. Phys.* **18**, 817 (1950)]. We propose a generalisation of Irving and Kirkwood's argument to fluctuating, non-planar surfaces and obtain an expression for the pressure tensor that is not smeared by thermal fluctuations at the molecular scale and corresponding capillary waves [F. P. Buff *et al.*, *Phys. Rev. Lett.* **15**, 621–623 (1965)]. We observe the emergence of surface tension, defined as an excess tangential stress, acting exactly across the dividing surface at the sharpest molecular resolution. The new statistical mechanical expressions extend current treatments to fluctuating inhomogeneous systems far from equilibrium. © 2018 Author(s). All article content, except where otherwise noted, is licensed under a Creative Commons Attribution (CC BY) license (<http://creativecommons.org/licenses/by/4.0/>). <https://doi.org/10.1063/1.5020991>

I. INTRODUCTION

Inhomogeneous systems are characterised by an interface, across which physical quantities vary sharply, over a length scale of a few molecular diameters.¹ Thermally induced fluctuations of the interface in the form of capillary waves smooth out the transition of properties across the interface. Although capillary wave behaviour has been observed experimentally,^{2,3} analysis of the interfacial structure at the sharpest molecular resolution is difficult as a result of these fluctuations. Capillary wave theory (CWT), introduced by Buff *et al.*,^{4,5} accounts for these by assuming the existence of an intrinsic surface $\xi(\mathbf{x})$, where \mathbf{x} is a vector in the coordinate system parallel to the surface. This function acts as an instantaneous boundary between fluid phases, against which statistical averages are computed, e.g., the intrinsic density profile,

$$\tilde{\rho}(z + \xi) = \frac{1}{A} \sum_{i=1}^N \langle \delta(z + \xi(\mathbf{x}_i) - z_i) \rangle, \quad (1)$$

where $(\mathbf{x}_i, z_i) = (x_i, y_i, z_i)$ are the atom positions and $A = L_x L_y$ is the transverse area. In its original form,⁴ CWT sees the interface at the largest wavelength as a step function, whose local position is described by a Gaussian distribution $P(\xi) \propto \exp(-(\xi - \langle \xi \rangle)^2 / 2w^2)$. The square width w^2 characterises the correlation length of the surface fluctuations and

is known to have the taxing property of, in the absence of an external field, diverging in the thermodynamic limit.^{6,7} The connection with the singlet density $\rho(z)$ is often accomplished by ignoring the coupling between capillary wave fluctuations and the interfacial structure, resulting in a congruent fluctuation of the intrinsic profile. The mean density profile is then obtained from the convolution over the capillary waves, $\rho(z) = \int d\xi \tilde{\rho}(z - \xi) P(\xi)$.⁸

Among the different results reported previously, the interfacial Hamiltonian approach (e.g., Refs. 9–12) gives useful information on the wavenumber dependence of surface tension but relies on various phenomenological parameters which are not known beforehand. Furthermore recently, there has been a renewed interest in the analysis of the pressure tensor in inhomogeneous systems, notably by Sega *et al.* in Ref. 13 for a Lennard-Jones (LJ) fluid and in Ref. 14 for molecular liquids. In these studies, the authors performed a deconvolution of the pressure tensor from the fluctuations in the interface position, thereby obtaining its intrinsic counterpart. The intrinsic profile of single particle properties is trivially obtained by appropriate weighting of the sum in Eq. (1), $\tilde{\rho}_w(z + \xi) = \sum_i \langle w_i \delta(z + \xi(\mathbf{x}_i) - z_i) \rangle / A$, where w_i is an arbitrary atomic weight. By contrast, the potential component of the pressure, $\mathbf{P}^c(\mathbf{r})$, is not easily defined due to the intermolecular interactions.¹⁵ For a pairwise potential, $\mathbf{P}^c(\mathbf{r}) = 1/2 \sum_{i \neq j} \langle \mathbf{F}_{ij} \int_{C_{ij}} d\mathbf{l} \delta(\mathbf{l} - \mathbf{r}) \rangle$, where \mathbf{F}_{ij} is the force between the pair of atoms and C_{ij} is the path of the line integral connecting atoms i and j .

There is no unique way of defining C_{ij} , and so there is also no unique way of determining which atom pairs contribute to the force across a given surface element.¹⁶

^{a)}ccorreia@imperial.ac.uk

^{b)}edward.smith05@imperial.ac.uk

^{c)}andreas.nold09@imperial.ac.uk

^{d)}d.n.sibley@lboro.ac.uk

^{e)}s.kalliadasis@imperial.ac.uk

The Irving-Kirkwood (IK) convention¹⁷ stipulates that the force between two atoms is said to be *across* if the vector connecting the centres of mass of the two atoms intersects the surface element. The alternative Harasima (H) contour¹⁸ breaks the line connecting a pair of atoms into two mutually orthogonal paths. For planar interfaces, the H representation is seen as particularly convenient because, by construction, the transverse contribution of each pair of particles becomes path independent;¹³ on the other hand, there are always two possible H contours connecting a pair of particles, first transverse and then normal $\uparrow\circ\rightarrow$, and vice versa, $\rightarrow\circ\uparrow$. In the presence of an interface, this distinction is important because it defines the position where the contribution to the total pressure is accounted for. This is usually mitigated by equally partitioning the contribution at each particle's location, but it does not resolve the fundamental ambiguity.

Furthermore, it is also recognised that the normal component of this contour is known not to be physically meaningful.^{13,19} This additional conceptual difficulty is usually reconciled by arguing that mechanical stability, $\nabla\cdot\mathbf{P} = 0$, requires uniformity of the normal pressure across the system. As it stands, this assumption can only hold under equilibrium conditions. Gradients in mass, momentum, and energy will generate thermodynamic fluxes that change the liquid structure, vis-à-vis the interfacial properties.^{20,21} Physical modeling of coupling between these is key to understanding the behaviour of fluids under non-equilibrium conditions. Examples include the suppression of thermal fluctuations by shear flow,^{22,23} Faraday instability at the liquid-vapour interface,²⁴ and Marangoni flow.²⁵

The motivation of this work is thus to extend the IK definition of the pressure tensor as a force acting across a non-planar surface, fluctuating as a result of the thermal motions of the fluid. Starting from the continuity equations of hydrodynamics, expressed relative to a fluctuating reference frame, new expressions are derived which are valid for any inhomogeneous fluid far from equilibrium. But unlike the H or IK line integrals, the new contour of integration is a dynamic quantity, reflecting the instantaneous local curvature of the interface. Using the control volume approach²⁶ to the IK equations, we compute the pressure profile of a well-known liquid-vapour LJ fluid. We find the emergence of the surface tension acting exactly across the intrinsic surface, free from the smearing effects of the surface separating the liquid and vapour phases.

II. INTRINSIC PRESSURE TENSOR

In its original form, the IK microscopic expressions for thermodynamic fluxes are written in terms of ensemble averages. Thermodynamic fluxes are, however, based on conservation laws, valid instantaneously over every member in the statistical ensemble. The Dirac delta functions become a convenient operator whose physical meaning only becomes apparent when averaging over the volume.²¹ We therefore drop the ensemble averaging of the density operators in our analysis following the procedure of Todd *et al.*^{15,20} The mass density $\rho(\mathbf{r}, t)$ and momentum density $\mathbf{J}(\mathbf{r}, t)$ are defined by

$$\rho(\mathbf{r}, t) = \sum_{i=1}^N m_i \delta(\mathbf{r} - \mathbf{r}_i(t)), \quad (2)$$

$$\mathbf{J}(\mathbf{r}, t) = \sum_{i=1}^N m_i \dot{\mathbf{r}}_i \delta(\mathbf{r} - \mathbf{r}_i(t)), \quad (3)$$

where m_i , \mathbf{r}_i , and $\dot{\mathbf{r}}_i$ are the particles' mass, position, and total velocity, respectively. Their hydrodynamic formulation²⁶ allows the densities to be expressed in control volume form rendering them more analytically tractable. Given a region of interest, the integral of the local density,

$$\int_V d\mathbf{r} \rho(\mathbf{r}, t) = \int_V d\mathbf{r} \sum_{i=1}^N m_i \delta(\mathbf{r} - \mathbf{r}_i), \quad (4)$$

is the total mass inside the control volume. The region interval is arbitrary as long as it is compact. Assuming that one can obtain the intrinsic surface $\xi(\mathbf{x})$ over the xy -plane for a given configuration, the volume can be foliated into regular elements

$$\int_V d\mathbf{r} = \int_{x^-}^{x^+} dx \int_{y^-}^{y^+} dy \int_{z^- + \xi(x,y)}^{z^+ + \xi(x,y)} dz = \Delta x \Delta y \Delta z, \quad (5)$$

where the limits of integration are defined as $\Delta\mathbf{r} = \mathbf{r}^+ - \mathbf{r}^-$. Here, we are interested in the distribution of the pressure as a function of the distance to the interface. This can be achieved by a change of coordinate system and, in accordance with CWT assumptions, we adopt the view that surface fluctuations are independent of interfacial structures. The arbitrary surface $\xi(\mathbf{x})$ is therefore taken to be independent of time, thereby avoiding the appearance of time dependent contributions to the pressure due to the dynamic motion of the surface. Integration of the operators $\delta(\mathbf{r} - \mathbf{r}_i)$ over the control volume has the effect of isolating the particles inside the region of interest,²⁶ and Eq. (4) expands to

$$\begin{aligned} \int_V d\mathbf{r} \rho(\mathbf{r}, t) &= \int_{x^-}^{x^+} dx \int_{y^-}^{y^+} dy \int_{z^- + \xi(x,y)}^{z^+ + \xi(x,y)} dz \sum_{i=1}^N m_i \delta(\mathbf{r} - \mathbf{r}_i) \\ &= \sum_{i=1}^N m_i \vartheta_{x_i} [x^-, x^+] \vartheta_{y_i} [y^-, y^+] \\ &\quad \times \vartheta_{z_i} [z^- + \xi(x_i, y_i), z^+ + \xi(x_i, y_i)], \end{aligned} \quad (6)$$

where the x and y integrals, in the last line, use the sifting property $\int_{-\infty}^{\infty} d\alpha f(\alpha) \delta(\alpha - \alpha_i) = f(\alpha_i)$; the boxcar function ϑ results from the integral of the Dirac delta between finite limits, $\vartheta_{\alpha_i} [\alpha^-, \alpha^+] \equiv \theta(\alpha^+ - \alpha_i) - \theta(\alpha^- - \alpha_i)$, $\alpha = x, y, z$, and $\theta(\alpha)$ is the Heaviside step function. Assuming periodic boundary conditions in the transverse directions, $\vartheta_{x_i} [0, L_x] = 1 \forall x_i \in (0, L_x)$ and $\vartheta_{y_i} [0, L_y] = 1 \forall y_i \in (0, L_y)$,

$$\int_V d\mathbf{r} \rho(\mathbf{r}, t) = \sum_{i=1}^N m_i \vartheta_{z_i} [z^- + \xi(\mathbf{x}_i), z^+ + \xi(\mathbf{x}_i)], \quad (7)$$

where $\mathbf{x}_i = (x_i, y_i)$. The mean value theorem applied on the left-hand side of Eq. (7) gives a measure of the volume

average density $\tilde{\rho}(z + \xi) \approx \int_V d\mathbf{r} \rho(\mathbf{r}, t) / \Delta V$, $z \in (z^-, z^+)$, with $\Delta V = A \Delta z$. Using the definition of the Dirac delta function in the zero volume limit, $\Delta z \rightarrow 0$, $\delta(z) \equiv \lim_{\Delta z \rightarrow 0} (\theta(z + \Delta z/2) - \theta(z - \Delta z/2)) / \Delta z$, the density at a given position relative to the surface, $z + \xi(\mathbf{x})$ is given by

$$\tilde{\rho}(z + \xi) = \frac{1}{A} \sum_{i=1}^N m_i \delta(z + \xi(\mathbf{x}_i) - z_i). \quad (8)$$

The above equation defines the instantaneous density relative to a given surface. Assuming that one can somehow compute $\xi(\mathbf{x})$, the average over the ensemble of configurations and corresponding surfaces is the intrinsic density profile, $\langle \tilde{\rho}(z + \xi) \rangle$.⁴ The above equation deserves particular emphasis because its derivation is based on a microscopic expression of a hydrodynamic quantity, without any assumption regarding the distribution function $f(\mathbf{r}^N, \mathbf{p}^N, t)$. It can therefore form the basis for a statistical mechanical derivation of the pressure tensor in a Lagrangian frame of reference relative to the instantaneous surface. Starting from the definition of momentum, Eq. (3), the same process can be followed to obtain an instantaneous momentum density relative to the surface,

$$\tilde{\mathbf{J}}(z + \xi) = \frac{1}{A} \sum_{i=1}^N m_i \dot{\mathbf{r}}_i \delta(z + \xi(\mathbf{x}_i) - z_i). \quad (9)$$

The time derivative of Eq. (3) at a given point results in the momentum conservation equation where,

for a system of pairwise interacting particles, the microscopic representation of the IK pressure tensor²¹ is given by

$$\mathbf{P}(\mathbf{r}, t) = \mathbf{P}^k(\mathbf{r}, t) + \mathbf{P}^c(\mathbf{r}, t) = \sum_{i=1}^N m_i \mathbf{v}_i \mathbf{v}_i \delta(\mathbf{r} - \mathbf{r}_i) + \frac{1}{2} \sum_{\substack{i,j=1 \\ i \neq j}}^N \mathbf{r}_{ij} \mathbf{F}_{ij} \int_0^1 d\lambda \delta(\mathbf{r} - \mathbf{r}_\lambda), \quad (10)$$

where $\mathbf{P}^k(\mathbf{r}, t)$ is the kinetic contribution to the pressure, obtained by decomposition of the total velocity $\dot{\mathbf{r}}_i$ into a thermal component \mathbf{v}_i and a streaming part $\mathbf{u}(\mathbf{r}_i, t)$, taken to be zero in the current work, $\dot{\mathbf{r}}_i = \mathbf{v}_i + \mathbf{u}(\mathbf{r}_i, t)$. Akin to density [cf. Eq. (2)] and momentum [cf. Eq. (3)], $\mathbf{P}^k(\mathbf{r}, t)$ is localised at the atom positions by $\delta(\mathbf{r} - \mathbf{r}_i)$. The configurational part of the pressure tensor, $\mathbf{P}^c(\mathbf{r}, t)$, is obtained by integrating along the line connecting a pair of atoms, where each point $\mathbf{r}_\lambda = \mathbf{r}_i - \lambda \mathbf{r}_{ij}$ is sampled by $\delta(\mathbf{r} - \mathbf{r}_\lambda)$. Starting from the IK form of the pressure in Eq. (10) and following the same procedure used to obtain intrinsic density above, we aim to obtain the IK pressure tensor mapped onto a coordinate system defined by the instantaneous intrinsic surface. The integral of the pressure tensor over a control volume bounded by a surface $\xi(\mathbf{x})$ is given by

$$\begin{aligned} \int_V d\mathbf{r} \mathbf{P}(\mathbf{r}, t) &= \int_{x^-}^{x^+} dx \int_{y^-}^{y^+} dy \int_{z^- + \xi(x,y)}^{z^+ + \xi(x,y)} dz \sum_{i=1}^N m_i \mathbf{v}_i \mathbf{v}_i \delta(\mathbf{r} - \mathbf{r}_i) + \frac{1}{2} \int_{x^-}^{x^+} dx \int_{y^-}^{y^+} dy \int_{z^- + \xi(x,y)}^{z^+ + \xi(x,y)} dz \sum_{\substack{i,j=1 \\ i \neq j}}^N \mathbf{r}_{ij} \mathbf{F}_{ij} \int_0^1 d\lambda \delta(\mathbf{r} - \mathbf{r}_\lambda) \\ &= \sum_{i=1}^N m_i \mathbf{v}_i \mathbf{v}_i \vartheta_{x_i} [x^-, x^+] \vartheta_{y_i} [y^-, y^+] \vartheta_{z_i} [z^- + \xi(x_i, y_i), z^+ + \xi(x_i, y_i)] \\ &\quad + \frac{1}{2} \sum_{\substack{i,j=1 \\ i \neq j}}^N \mathbf{r}_{ij} \mathbf{F}_{ij} \int_0^1 d\lambda \vartheta_{x_\lambda} [x^-, x^+] \vartheta_{y_\lambda} [y^-, y^+] \vartheta_{z_\lambda} [z^- + \xi(x_\lambda, y_\lambda), z^+ + \xi(x_\lambda, y_\lambda)], \end{aligned} \quad (11)$$

where x_λ , y_λ , and z_λ are the components of a point in the vector connecting particles i and j . The integral of λ from 0 to 1 moves along the line and partitions the energy between the different volume elements across which the contour line passes through. This seemingly complicated looking function has the clear geometric meaning that the path between each pair of particles is not a straight line but a curve—unique to each pair of interacting particles—whose coordinates are dictated by the shape of the interface at the transversal coordinates x_λ and y_λ . Approximating the energy in Eq. (11) by its volume average, $\tilde{\mathbf{P}}(z + \xi) \approx \int_V d\mathbf{r} \mathbf{P}(\mathbf{r}, t) / \Delta V$, over the xy -plane, and using the Heaviside definition of the Dirac delta function when $\Delta z \rightarrow 0$, the instantaneous pressure relative to the surface is given by

$$\begin{aligned} \tilde{\mathbf{P}}(z + \xi) &= \tilde{\mathbf{P}}^k(z + \xi) + \tilde{\mathbf{P}}^c(z + \xi) \\ &= \frac{1}{A} \sum_{i=1}^N m_i \mathbf{v}_i \mathbf{v}_i \delta(z + \xi(\mathbf{x}_i) - z_i) \\ &\quad + \frac{1}{2A} \sum_{\substack{i,j=1 \\ i \neq j}}^N \mathbf{r}_{ij} \mathbf{F}_{ij} \int_0^1 d\lambda \delta(z + \xi(\mathbf{x}_\lambda) - z_\lambda), \end{aligned} \quad (12)$$

where $\mathbf{x}_\lambda = (x_\lambda, y_\lambda)$ are the coordinates of the line between a pair of particles transversal to the interface. In the particular case where the intrinsic surface is planar, $\xi(\mathbf{x}) = c$, which can be absorbed into the coordinate position z , and the above equation gives the IK expression for the pressure tensor, Eq. (10),

averaged over the xy -plane,

$$\begin{aligned} \tilde{\mathbf{P}}(z) = \tilde{\mathbf{P}}^k(z) + \tilde{\mathbf{P}}^c(z) = & \frac{1}{A} \sum_{i=1}^N m_i \mathbf{v}_i \mathbf{v}_i \delta(z - z_i) \\ & + \frac{1}{2A} \sum_{\substack{i,j=1 \\ i \neq j}}^N \mathbf{r}_{ij} \mathbf{F}_{ij} \int_0^l d\lambda \delta(z - z_{i\lambda}). \end{aligned} \quad (13)$$

Equation (12) is the main result of the current work. Unlike the IK and H conventions, the contour line for each pair of particles is a unique path that reflects the local curvature of the instantaneous interface, setting the current analysis apart from previous studies.^{13,14,27,28} Its average over an ensemble of configurations gives a precise definition of the intrinsic pressure tensor, $\tilde{\mathbf{P}}(z + \xi) = \langle \mathbf{P}(z + \xi) \rangle$, free from the smearing effect of surface fluctuations. Because its foundations are hydrodynamic, it is not bound to any equilibrium distribution, thereby paving the way to the study of complex fluids under non-equilibrium conditions.

III. SIMULATION OF LIQUID-VAPOUR INTERFACE

A. Intrinsic pressure and surface tension

We apply Eq. (12) to the analysis of a liquid-vapour interface of a simple LJ fluid. Surface tension is the defining physical property characterizing the interfacial structure. From a mechanical standpoint, it arises from the anisotropy of the pressure tensor, reflecting the distinct way molecular interactions vary across the system,

$$\gamma = \lim_{l \rightarrow \infty} \int_{-l}^l dz (P_N(z) - P_T(z)), \quad (14)$$

where P_N , and P_T are the components of the pressure tensor normal and transverse to the surface (assuming cylindrical symmetry). The link between these two approaches is given by the principle of virtual work, summarised here for completeness. Given a fluid element $dV = L_x L_y dz = Adz$ and a deformation tensor given by $\epsilon_{xx} = \epsilon_{yy} = (1 + \epsilon)$, $\epsilon_{zz} = 1/(\epsilon_{xx} \epsilon_{yy})$, and $\epsilon_{\alpha\beta} = 0$, $\alpha \neq \beta$ and then to first order in the Cauchy strain ϵ , the change in area is $\delta A = 2 \epsilon A$ and the work done by the system is

$$\delta W = \epsilon L_x L_y dz (P_x(z) + P_y(z) - 2P_z(z)). \quad (15)$$

By virtue of its definition, the transformation preserves the volume, so the free energy cost per unit area is $\delta F/\delta A = dz (P_N(z) - P_T(z))$, where $P_N = P_z$ and $P_T = (P_x + P_y)/2$. This analysis merits some justification: (i) the approximation is only valid for infinitesimal deformations $\epsilon \ll 1$, hinting at the fact that surface tension is an equilibrium property, and (ii) any excess pressure in the transversal direction will cost energy wherever its position across the system. What is perhaps unnoticed from this argument is that gradients in density may break the symmetry of the pressure components and are bound to create tension in the direction transversal to the interface. Although this has been observed previously,¹³ one aim of the current study is to quantitatively analyze in detail this

behaviour across the interfacial region. In accordance with CWT, taking the interface at the longest wavelength, we can use Eq. (12) to decouple the capillary wave fluctuations and use it to analyze the molecular origins of the surface tension at the interface,

$$\tilde{\gamma} = \lim_{l \rightarrow \infty} \int_{-l}^l dz (\tilde{P}_N(z) - \tilde{P}_T(z)). \quad (16)$$

B. Molecular dynamics simulations

Molecular dynamics (MD) simulations of a liquid-vapour interface are performed with a system of $N = 6000$ particles inside a simulation cell of dimensions $L_x = L_y = 14.0$ and $L_z = 80.0$, where unless otherwise indicated, reduced units are used throughout this work. The system size was chosen to be larger than the minimum value of $N = 1000$ particles as illustrated by Trokhymchuk *et al.*²⁹ The shorter dimension of the simulation box was chosen to be larger than $L_x \approx 10$ to avoid spurious correlations in the interface fluctuations,³⁰ and a longer dimension $L_z > 5L_x$ was chosen to avoid coupling between the two interfaces in the system. Atoms interact through a spherical truncated and shifted LJ potential with a cutoff radius of $r_{cut} = 2.5$,

$$\phi(r) = 4\epsilon \left[\left(\frac{\sigma}{r} \right)^{12} - \left(\frac{\sigma}{r} \right)^6 \right] - 4\epsilon \left[\left(\frac{\sigma}{r_{cut}} \right)^{12} - \left(\frac{\sigma}{r_{cut}} \right)^6 \right], \quad r < r_{cut}, \quad (17)$$

where r is the distance between a pair of particles and the corresponding energy and length scales are defined by $\epsilon = 1$ and $\sigma = 1$, respectively.

Two temperatures are considered, $T = 0.6$ and $T = 0.7$. These were chosen to emphasise the effects of a dense fluid with a sharp liquid-vapour interface. Although different values of the triple point temperature of a LJ fluid have been reported (e.g., Mastny and de Pablo give a value of $T = 0.694$,³¹ while Errington *et al.*³² report a value of $T = 0.560$ using the same cutoff as the current work), it has been shown previously³³ that the current pair radial distribution functions of the studied systems do not exhibit evidence of solid-phase structures. The equations of motion are integrated using the LAMMPS (Large-scale Atomic/Molecular Massively Parallel Simulator) software package.³⁴ The temperature is controlled with a Nosé-Hoover^{35,36} thermostat with mass $m_\eta = 50.0$. For each temperature, 200 statistically independent trajectories are equilibrated for 5×10^5 steps using a time step $\Delta t = 0.001$. After equilibration, 50 configurations are sampled from each trajectory every 10^4 time steps over further 5×10^5 steps giving a total set of 10^4 configurations over which statistical analysis of the interfacial properties is performed.

C. Intrinsic surface analysis

Analysis of the interfacial region at the molecular scale requires an operational definition of the collective coordinates of the intrinsic surface $\xi(\mathbf{x})$ for a given molecular configuration. This step is accomplished through a percolation analysis to separate the liquid phase—identified by the spanning cluster—from the isolated clusters in the vapour phase. Originally put forward by Stillinger,³⁷ several approaches have been developed to this end.^{38–45} In

particular, the intrinsic sampling method (ISM) was the first implementation allowing a quantitative comparison between computer simulations and CWT^{38,39} and is the method of choice in the current analysis. The ISM can be interpreted as an outlier detection method⁴⁶ that iteratively estimates the amplitudes of a Fourier series representation of the intrinsic surface,

$$\xi(\mathbf{x}; k_u) = \sum_{|\mathbf{k}| \leq k_u} \hat{\xi}_{\mathbf{k}} e^{i\mathbf{k} \cdot \mathbf{x}}, \quad (18)$$

where $\mathbf{x} = (x, y)$ is a vector parallel to the surface, $\hat{\xi}_{\mathbf{k}}$ are the amplitudes associated with each wavevector in the basis set, $\mathbf{k} = 2\pi(n_x/L_x, n_y/L_y)$, with $n_x, n_y = 0, \pm 1, \pm 2, \dots$, and $k_u = 2\pi/\lambda_u$ is an upper wavevector cutoff that sets the lower resolution limit λ_u of the surface. Here the judicious choice within CWT is to set a cutoff wavelength commensurate with the molecular size $\lambda_u \approx \sigma$.³⁸ A basic assumption behind ISM is that the molecular system consists of a set of surface atoms, or *inliers*, whose position is described by the assumed mathematical model, Eq. (18), and *outliers*—representing the atoms in the liquid and vapour phases—which are not accounted by the model. The spanning cluster is obtained by a graph traversal algorithm that identifies the largest set of atoms with at least 3 neighbours at distances below 1.4. From this set, an initial estimate of the surface *inliers* is obtained by dividing the xy -plane into a 3×3 mesh and finding the $N_s = 9$ atoms with the largest z coordinate in each mesh element. The intrinsic surface is then defined as the surface of least area passing through the selected atoms. This is accomplished by minimizing the objective function

$$\min_{|\mathbf{k}| \leq k_u} f(\hat{\xi}_{\mathbf{k}}) \equiv \frac{\omega}{2} \sum_{i=1}^{N_s} (z_i - \xi(\mathbf{x}_i))^2 + \frac{A}{2} \sum_{|\mathbf{k}| \leq k_u} \mathbf{k}^2 |\hat{\xi}_{\mathbf{k}}|^2, \quad (19)$$

where $A = L_x L_y$ and ω is a constant that specifies the strength of the harmonic restraints tethering the surface to the atomic positions. The method then searches the percolating cluster for the closest atom to the minimal surface that is not part of the set of *inliers*. The procedure is iterated until an optimum value of the surface density $n_s = N_s/A$ is reached. At the highest level of resolution, the surface atoms are represented in the density profile as a delta function $n_s \delta(z)$. Too low a value of n_s results in a unphysical shoulder between the surface and the first layer in the liquid phase of the intrinsic density profile $\tilde{\rho}(z)$, and too large values are characterised by a degenerate mathematical surface that tries to fit all the surface atoms.⁴⁷ For the LJ system at the studied temperatures, it was found $n_s = 0.8$ to best describe the interface at the molecular scale with a clear peak at the origin followed by a significant oscillatory structure whose amplitude decays toward the liquid bulk density.

IV. RESULTS

Figure 1 depicts the intrinsic profiles at $T = 0.6$ and $T = 0.7$, respectively, obtained using the largest wavevector cutoff $k_u = 2\pi$. Intrinsic quantities are plotted in a frame centred on the intrinsic surface, with the corresponding fixed grid quantities centred on the location of the appropriate Gibbs dividing surface. For convenience, both surfaces are denoted as being

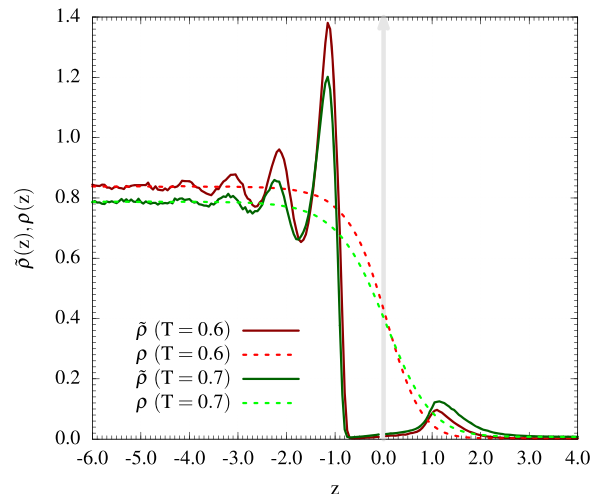


FIG. 1. Intrinsic density profiles $\tilde{\rho}(z)$ (solid line) compared to mean density $\rho(z)$ (dashed line) for systems at $T = 0.6$ (red) and $T = 0.7$ (green), respectively. Surface atoms are represented by the delta function, represented as a gray arrow at $z = 0$. The mean density profiles were centred at their corresponding Gibbs dividing surfaces $\langle \xi \rangle$.

at $z = 0$ in Fig. 1, and this convention is followed for all other figures (Figs. 1–4) in this work. The removal of the blurring effect of thermal fluctuations results in the clear appearance of the molecular structure at the interface, given by the delta-function at $z = 0$ representing the surface layer, followed by a strong oscillatory structure whose amplitude decays to zero at the bulk liquid density, and an adsorption peak at $z \approx 1.0$ in agreement with previous results.^{47,48}

The kinetic and configurational components of the intrinsic pressure profile [cf. Eq. (12)] at $T = 0.6$ are depicted in Fig. 2. The dyadic terms $m_i \mathbf{v}_i \mathbf{v}_i$ in the kinetic component $\tilde{\mathbf{P}}^k$, being a single particle property, are as a result directly proportional to the intrinsic density through the kinetic equation of state $\tilde{P}^k(z) = \tilde{\rho}(z) k_B T$, where k_B is Boltzmann's constant.

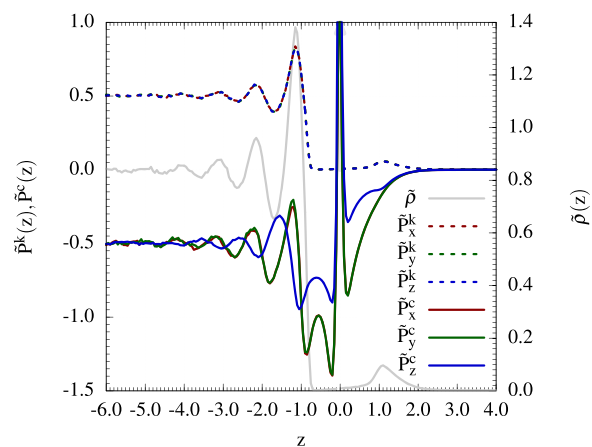


FIG. 2. Kinetic and configurational components of the intrinsic pressure tensor, $\tilde{\mathbf{P}}^k(z)$ and $\tilde{\mathbf{P}}^c(z)$, at $T = 0.6$. At constant temperature, \tilde{P}_x^k (dashed red), \tilde{P}_y^k (dashed green), and \tilde{P}_z^k (dashed blue) are identical and proportional to the intrinsic density. Cylindrical symmetry about the normal axis gives identical configurational terms parallel to the interface, \tilde{P}_x^c (red line) and \tilde{P}_y^c (green line), within statistical uncertainty. The configurational pressure normal to the interface, \tilde{P}_z^c (blue line), is significantly larger in the intermediate regions between the peaks the intrinsic density profile. The intrinsic density, $\tilde{\rho}(z)$ (gray line), is plotted on the secondary vertical axis.

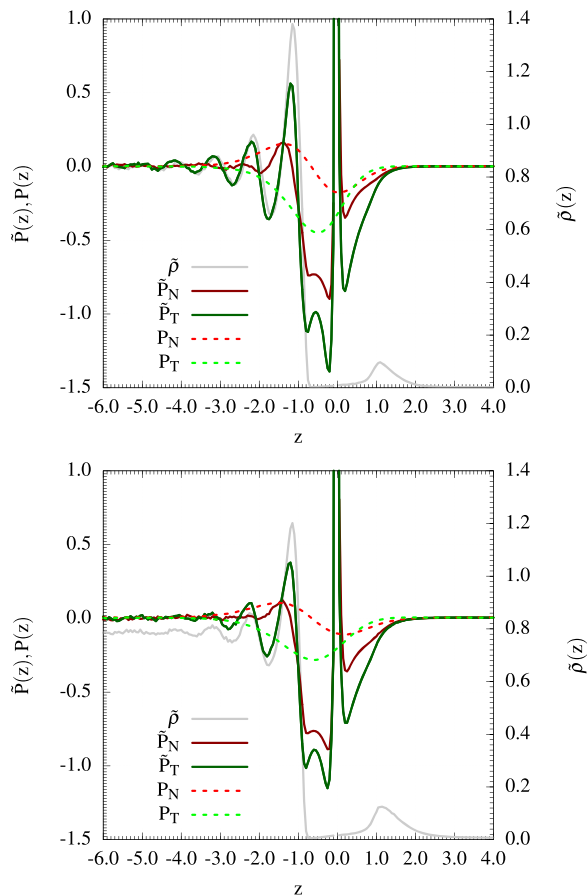


FIG. 3. Top panel: components of the intrinsic pressure tensor normal, $\tilde{P}_N = \tilde{P}_z$ (red), and transversal to the interface, $\tilde{P}_T = (\tilde{P}_x + \tilde{P}_y)/2$ (green), at $T = 0.6$. The mean profiles P_N (dashed red line) and P_T (dashed green line) are plotted for comparison. The intrinsic density, $\tilde{\rho}(z)$ (gray), is plotted on the secondary vertical axis. Bottom panel: intrinsic and average pressure profiles normal and transversal to the interface at $T = 0.7$. The notation is the same as the top panel.

At constant temperature, these are all equal, emphasising the well-known fact that, in the absence of temperature gradients, surface tension is a configurational property as attested by the configurational terms $\tilde{\mathbf{P}}^c$.⁴⁹ On the liquid phase, away from the interface (viz., $z \lesssim -4.0$), these are equivalent by a symmetry argument, i.e., the configurational pressure tensor is isotropic (the negative value reflects the cohesive energy of the LJ interactions).

In the layers closer to the interface, fluctuations in density break the symmetry of interactions. Figure 3 illustrates this difference in more detail for $\tilde{P}_N = \tilde{P}_z$ and $\tilde{P}_T = (\tilde{P}_x + \tilde{P}_y)/2$, at $T = 0.6$ and $T = 0.7$, respectively. The transverse pressure \tilde{P}_T follows closely the oscillations in density, supporting the notion that, at the peaks in the intrinsic density, the larger number of neighbours interacting with an atom in the directions parallel to the interface results in a higher proportion of short ranged repulsive interactions contributing to the extra stress.

On the other hand, in the normal direction, \tilde{P}_N exhibits a more steady profile up until the region between the first two layers in the liquid phase. While being zero at the peak locations, reflecting mechanical equilibrium of the liquid layers (cf. Fig. 3, viz., $z \approx -1 \times 2^{1/6}$ and $z \approx -2 \times 2^{1/6}$), there is a clear positive excess normal pressure between these at

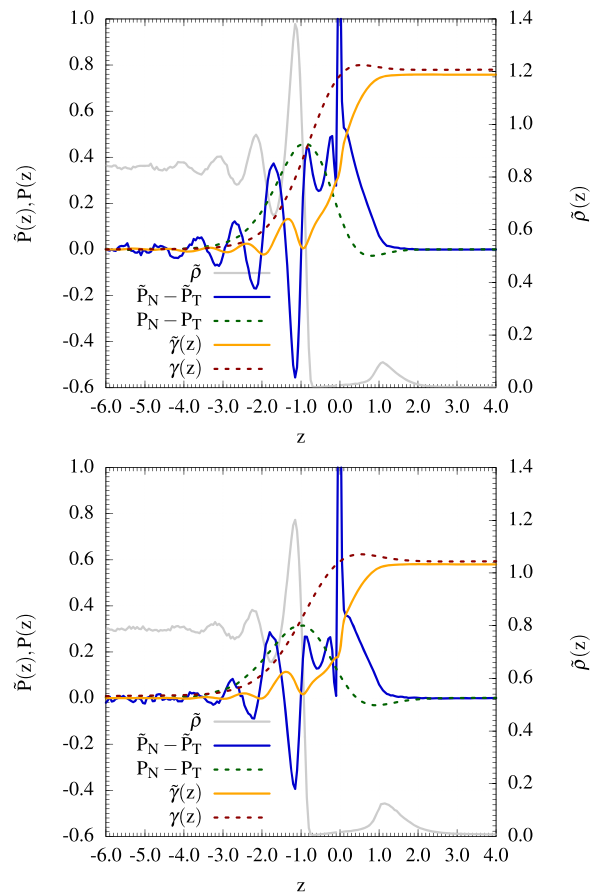


FIG. 4. Top panel: comparison between excess intrinsic pressure, $\tilde{P}_N - \tilde{P}_T$ (blue), and its mean counterpart (green) at $T = 0.6$. The bottom panel shows the results at $T = 0.7$. The notation is the same as the top panel.

$z \approx 1.5$. The physical argument behind this excess energy resides in the observation that an atom located at this position would experience the short range repulsive forces of the adjacent fluid layers. The resultant instability would force the atom to transit to one of the layers, thus preserving the liquid structure next to the interface.

We note that at larger distances from the interface, the mean normal pressure P_N is equal in the liquid and vapour phase, as can be seen in Fig. 3. Over the surface, the mean divergence of the pressure will still be equal to zero; i.e., mechanical equilibrium must be satisfied as the surface is stationary.

Figure 4 depicts the excess pressure of the fluid, defined by $\tilde{P}_N(z) - \tilde{P}_T(z)$, whose integral over the entire domain, $\gamma(z) = \int_{-\infty}^z dz' (P_N(z') - P_T(z'))$, gives the Kirkwood-Buff⁵⁰ definition of the surface tension [cf. Eqs. (15) and (16)]. At the highest molecular resolution, the intrinsic pressure tensor Eq. (12) allows us to ascertain the microscopic mechanism involved in giving rise to the interfacial energy.

We can observe that the surface tension has contributions from both the liquid and vapour facing sides of the (intrinsic) interface. Importantly, however, we note that the depletion region between the first layer of fluid at the surface layer is precisely where the onset of the surface tension takes place. We are also able to see that the adsorption peak—approximately one fluid layer away from the surface—is vital to the contribution

of the other half of the surface tension. Crucially, this is truly an adsorption peak rather than a density oscillation around the bulk vapour density (in contrast to the liquid facing side of the interface), due to the attraction of the vapour particles to the liquid (of course, as they are the same atoms). As the density increases and returns to the bulk vapour density, there is a net additive contribution to surface tension.

The physical picture is thus as follows: the surface tension, unlike the traditional mechanical picture—defined as the excess pressure acting across a surface of zero width between the liquid and vapour phases—arises instead across a boundary region spanning the three key layers involved in the intrinsic surface—the adsorbed layer at $z \approx 1.0$, the surface layer at $z = 0$, and the first layer in the liquid phase at $z \approx -1.0$. This region is constructed by pairs of layers attracting each other in an interleaved manner, at a distance commensurate with the attractive tail of the Lennard-Jones potential—the adsorbed layer at $z \approx 1.0$ with the first liquid layer at $z \approx -1.0$ and the surface layer at $z = 0$ with the second liquid layer at $z \approx -2.0$.

The results shown in Fig. 4 demonstrate that the surface tension force has similar contributions on either side of the interface, an observation first given in Ref. 13 but shown here with unprecedented clarity using the intrinsic pressure derived in this work.

V. CONCLUSION

We have proposed a generalisation of Irving and Kirkwood's expression for the pressure tensor free from the smearing effect of thermal fluctuations of capillary waves. This is accomplished by letting the contour of integration become a dynamic quantity, unique to each pair of interacting particles, that reflects the instantaneous local curvature of the interface. Expressing hydrodynamic fields in the control volume format, we are able to compute the intrinsic density profile that matches the profiles reported previously.

Applying the same technique to pressure allows the derivation of an intrinsic pressure tensor, which gives unprecedented insight into the liquid-vapour interface. More importantly, however, the notion of a mathematical surface of infinitesimal width, central to the mechanical definition of the surface tension, loses meaning at the microscopic level where the discrete nature of matter becomes apparent. Instead, we observe the emergence of the surface tension over a finite range of three atomic layers, acting exactly across the intrinsic surface.

The surface tension and other quantities of interest are derived from the continuity equations of hydrodynamics—expressed in a Lagrangian frame of reference relative to the intrinsic surface—and therefore are valid arbitrarily far from equilibrium. This makes the derived expressions particularly useful to the study of non-equilibrium inhomogeneous systems—e.g., Marangoni-driven flows, hydrodynamic instabilities, and bubble nucleation—which are inherently non-local and unsteady. Of particular interest would also be extension of this study to systems in confinement including heterogeneous substrates and nanochannels (e.g., Refs. 51 and 52).

ACKNOWLEDGMENTS

We acknowledge financial support from the European Research Council (ERC) through Advanced Grant No. 247031 and by the Engineering and Physical Sciences Research Council (EPSRC) of the UK through Grant No. EP/L020564.

- ¹J. S. Rowlinson and B. Widom, *Molecular Theory of Capillarity*, Dover Books on Chemistry (Dover Publications, 2002).
- ²M. K. Sanyal, S. K. Sinha, K. G. Huang, and B. M. Ocko, "X-ray-scattering study of capillary-wave fluctuations at a liquid surface," *Phys. Rev. Lett.* **66**, 628–631 (1991).
- ³I. M. Tidswell, T. A. Rabedeau, P. S. Pershan, and S. D. Kosowsky, "Complete wetting of a rough surface: An x-ray study," *Phys. Rev. Lett.* **66**, 2108–2111 (1991).
- ⁴F. P. Buff, R. A. Lovett, and F. H. Stillinger, Jr., "Interfacial density profile for fluids in the critical region," *Phys. Rev. Lett.* **15**, 621–623 (1965).
- ⁵R. Evans, "The nature of the liquid-vapour interface and other topics in the statistical mechanics of non-uniform, classical fluids," *Adv. Phys.* **28**, 143–200 (1979).
- ⁶J. R. Percus, in *Fluid Interfacial Phenomena*, Wiley-Interscience Publication, edited by C. A. Croxton (Wiley, 1986).
- ⁷E. M. Fernández, E. Chacón, P. Tarazona, A. O. Parry, and C. Rascón, "Intrinsic fluid interfaces and nonlocality," *Phys. Rev. Lett.* **111**, 096104 (2013).
- ⁸M. Müller and G. Münster, "Profile and width of rough interfaces," *J. Stat. Phys.* **118**, 669–686 (2005).
- ⁹K. R. Mecke and S. Dietrich, "Effective Hamiltonian for liquid-vapour interfaces," *Phys. Rev. E* **59**, 6766–6784 (1999).
- ¹⁰A. O. Parry, C. Rascón, and A. J. Wood "Critical effects at 3D wedge filling," *Phys. Rev. Lett.* **85**, 345 (2000).
- ¹¹F. Höfling and S. Dietrich, "Enhanced wavelength-dependent surface tension of liquid-vapour interfaces," *Europhys. Lett.* **109**, 46002 (2015).
- ¹²P. Yatsyshin, A. O. Parry, and S. Kalliadasis, "Complete prewetting," *J. Phys.: Condens. Matter* **28**, 275001 (2016).
- ¹³M. Sega, B. Fábíán, and P. Jedlovský, "Layer-by-layer and intrinsic analysis of molecular and thermodynamic properties across soft interfaces," *J. Chem. Phys.* **143**, 114709 (2015).
- ¹⁴M. Sega, B. Fábíán, G. Horvai, and P. Jedlovský, "How is the surface tension of various liquids distributed along the interface normal?," *J. Phys. Chem. C* **120**, 27468–27477 (2016).
- ¹⁵B. D. B. Todd, D. D. J. Evans, and P. P. J. Daivis, "Pressure tensor for inhomogeneous fluids," *Phys. Rev. E* **52**, 1627 (1995).
- ¹⁶M. Baus and R. Lovett, "Generalization of the stress tensor to nonuniform fluids and solids and its relation to Saint-Venants strain compatibility conditions," *Phys. Rev. Lett.* **65**, 1781–1783 (1990).
- ¹⁷J. H. Irving and J. G. Kirkwood, "The statistical mechanical theory of transport processes. IV. The equations of hydrodynamics," *J. Chem. Phys.* **18**, 817 (1950).
- ¹⁸A. Harasima, "Molecular theory of surface tension," *Adv. Chem. Phys.* **1**, 203–237 (1958).
- ¹⁹P. Schofield and J. R. Henderson, "Statistical mechanics of inhomogeneous fluids," *Proc. R. Soc. A* **379**, 231–246 (1982).
- ²⁰B. D. Todd and P. J. Daivis, *Mol. Simul.* **33**, 189–229 (2007).
- ²¹D. J. Evans and G. Morriss, *Statistical Mechanics of Nonequilibrium Liquids*, Theoretical Chemistry (Cambridge University Press, 2008).
- ²²D. Derks, D. G. A. L. Aarts, D. Bonn, H. N. W. Lekkerkerker, and A. Imhof, "Suppression of thermally excited capillary waves by shear flow," *Phys. Rev. Lett.* **97**, 038301 (2006).
- ²³M. Thiébaud and T. Bickel, "Nonequilibrium fluctuations of an interface under shear," *Phys. Rev. E* **81**, 1–13 (2010).
- ²⁴N. Francois, H. Xia, H. Punzmann, P. W. Fontana, and M. Shats, "Wave-based liquid-interface metamaterials," *Nat. Commun.* **8**, 14325 (2017).
- ²⁵A. Miniewicz, S. Bartkiewicz, H. Orlikowska, and K. Dradrach, "Marangoni effect visualized in two-dimensions optical tweezers for gas bubbles," *Sci. Rep.* **6**, 34787 (2016).
- ²⁶E. R. Smith, D. M. Heyes, D. Dini, and T. A. Zaki, "Control-volume representation of molecular dynamics," *Phys. Rev. E* **85**, 056705 (2012).
- ²⁷R. J. Hardy, "Formulas for determining local properties in molecular-dynamics simulations: Shock waves," *J. Chem. Phys.* **76**, 622 (1982).
- ²⁸J. F. Lutsko, "Stress and elastic constants in anisotropic solids: Molecular dynamics techniques," *J. Appl. Phys.* **64**, 1152–1154 (1988).

- ²⁹A. Trokhymchuk and J. Alejandre, "Computer simulations of liquid/vapor interface in Lennard-Jones fluids: Some questions and answers," *J. Chem. Phys.* **111**, 8510 (1999).
- ³⁰F. Bresme, E. Chacón, P. Tarazona, and K. Tay, "Intrinsic structure of hydrophobic surfaces: The oil-water interface," *Phys. Rev. Lett.* **101**, 056102 (2008).
- ³¹E. A. Mastny and J. J. de Pablo, "Melting line of the Lennard-Jones system, infinite size, and full potential," *J. Chem. Phys.* **127**, 104504 (2007).
- ³²J. R. Errington, P. G. Debenedetti, and S. Torquato, "Quantification of order in the Lennard-Jones system," *J. Chem. Phys.* **118**, 2256–2263 (2003).
- ³³C. Braga, J. Muscatello, G. Lau, E. A. Müller, and G. Jackson, "Nonequilibrium study of the intrinsic free-energy profile across a liquid-vapour interface," *J. Chem. Phys.* **144**, 044703 (2016).
- ³⁴S. Plimpton, "Fast parallel algorithms for short range molecular dynamics," *J. Comput. Phys.* **117**, 1–19 (1995).
- ³⁵W. Hoover, "Canonical dynamics: equilibrium phase-space distributions," *Phys. Rev. A* **31**, 1695–1697 (1985).
- ³⁶S. Nosé, "A molecular dynamics method for simulations in the canonical ensemble," *Mol. Phys.* **52**, 255–268 (1984).
- ³⁷F. H. Stillinger, "Capillary waves and the inherent density profile for the liquid–vapor interface," *J. Chem. Phys.* **76**, 1087–1091 (1982).
- ³⁸E. Chacón and P. Tarazona, "Intrinsic profiles beyond the capillary wave theory: A Monte Carlo study," *Phys. Rev. Lett.* **91**, 166103 (2003).
- ³⁹P. Tarazona and E. Chacón, "Monte Carlo intrinsic surfaces and density profiles for liquid surfaces," *Phys. Rev. B* **70**, 235407 (2004).
- ⁴⁰J. Chowdhary and B. M. Ladanyi, "Surface fluctuations at the liquid-liquid interface," *Phys. Rev. E* **77**, 1–14 (2008).
- ⁴¹M. Jorge and M. N. D. S. Cordeiro, "Intrinsic structure and dynamics of the water/nitrobenzene interface," *J. Phys. Chem. C* **111**, 17612–17626 (2007).
- ⁴²L. B. Pártay, G. Hantal, P. Jedlovsky, Á. Vincze, and G. Horvai, "A new method for determining the interfacial molecules and characterizing the surface roughness in computer simulations. Application to the liquid–vapor interface of water," *J. Comput. Chem.* **29**, 945–956 (2008).
- ⁴³M. Jorge, P. Jedlovsky, and M. N. D. S. Cordeiro, "A critical assessment of methods for the intrinsic analysis of liquid interfaces. 1. Surface site distributions," *J. Phys. Chem. C* **114**, 11169–11179 (2010).
- ⁴⁴M. Sega, S. S. Kantorovich, P. Jedlovsky, and M. Jorge, "The generalized identification of truly interfacial molecules (ITIM) algorithm for nonplanar interfaces," *J. Chem. Phys.* **138**, 044110 (2013).
- ⁴⁵A. P. Willard and D. Chandler, "Instantaneous liquid interfaces," *J. Phys. Chem. B* **114**, 1954–1958 (2010).
- ⁴⁶P. Rousseeuw and A. Leroy, *Robust Regression and Outlier Detection*, Wiley Series in Probability and Statistics (Wiley, 2005).
- ⁴⁷E. Chacón, E. Fernández, D. Duque, R. Delgado-Buscalioni, and P. Tarazona, "Comparative study of the surface layer density of liquid surfaces," *Phys. Rev. B* **80**, 195403 (2009).
- ⁴⁸E. Chacón and P. Tarazona, "Characterization of the intrinsic density profiles for liquid surfaces," *J. Phys.: Condensed Matter* **17**, S3493–S3498 (2005).
- ⁴⁹J. G. Kirkwood and F. P. Buff, "The statistical mechanical theory of surface tension," *J. Chem. Phys.* **17**, 338 (1949).
- ⁵⁰J. G. Kirkwood and F. P. Buff, "The statistical mechanical theory of solutions. I," *J. Chem. Phys.* **19**, 774 (1951).
- ⁵¹P. Yatsyshin, A. O. Parry, C. Rascón, and S. Kalliadasis, "Classical density functional study of wetting transitions on nanopatterned surfaces," *J. Phys.: Condens. Matter* **29**, 094001 (2017).
- ⁵²M. Morciano, M. Fasano, A. Nold, C. Braga, P. Yatsyshin, D. N. Sibley, B. D. Goddard, E. Chiavazzo, P. Asinari, and S. Kalliadasis, "Nonequilibrium molecular dynamics simulations of nanoconfined fluids at solid-liquid interfaces," *J. Chem. Phys.* **146**, 244507 (2017).